Journal of Sound and Vibration (1999) **219**(1), 105–132
Article No. jsvi.1998.1870, available online at http://www.idealibrary.com.on IDEAL

SCATTERING AT RIGID BUILDING CORNERS

F. P. MECHEL
Landhausstrasse 12, *D*-71120 *Grafenau* 1, *Germany*

(*Received* 12 *May* 1998, *and in final form* 20 *July* 1998)

In this paper the topic of two precedent papers [1, 2] (*Journal of Sound and Vibration* **216**, 649–671, 673–696), about sound fields in wedge-shaped spaces, is resumed and continued. Whereas the wedge angle in reference [1] is restricted to small values (below about 15°) and in reference [2] to medium values (below about 50°), the wedge space now is obtuse. As a further difference from the precedent papers, where the flanks of the wedge are absorbing, they are rigid in the present paper. It will be shown how sound sources are introduced into the field analysis, and how the singularity of the field in the wedge apex can be treated. Both sub-tasks are common to the theories for other wedge angle ranges, when the sound field is synthesized with wedge modes. A field of application of the present theory is the sound scattering by building corners and the noise shielding by buildings. When noise maps of the traffic noise in cities or of industrial noise in industrial plants need to be drawn, such scattering computations must be performed in a very great number of such cases. Therefore it is a task of this contribution to cast the results of the analytical evaluation into a form which is easily computed.

1. INTRODUCTION

The present paper is a member of a series of previous papers [1, 2] and of forthcoming papers which all have as their common topic the sound field analysis in wedge-shaped spaces. The common aim is the field synthesis with wedge modes, which are mutually orthogonal between the wedge flanks. The first contribution [1] displayed the reasons for the special difficulties which are encountered in wedge-shaped spaces and a solution was derived for small wedge angles Θ_0 (below about 15°). In the second contribution [2] the wedge was replaced by a cascade of straight duct sections and therefore it is limited to medium wedge angles (below about 50°). In both preceding papers the wedge flanks may be lined with locally reacting absorbers. The present paper is concerned with conditions of ideally reflecting flanks (either rigid or soft or mixed) which, as shown in reference [1], allows an easy modal analysis to be performed with "ideal wedge modes". The reasons for this paper are twofold. First, it shall be shown in the "easy environment" of ideal modes how sound sources in the wedge space are introduced into the analysis, and how the problems with the singular wedge apex can be handled, if the apex belongs to the sound field region. Both sub-tasks are common

0022–460X/99/010105 + 28 $30.00/0

to many other tasks in wedge-shaped spaces, when they are treated by a modal analysis.

Second, the present analysis has an eminently important application. Because the wedge angle may have any value $0 < \Theta_0 \leqslant 2\pi$, the present analysis can be applied also for obtuse wedge spaces as they are formed by building corners; see Figure 1. The scattering of sound by building corners and the shielding of noise by buildings (for sound propagation in a vertical plane *over* the building as well as in a horizontal plane *around* the building) evidently play important roles in the prediction of noise in urban environments and near industrial plants. In such predictions the noise level reduction by buildings must very often be computed. The analytical results displayed below for the corner scattering—although they are much simpler than the results in references [1, 2]—would need too long computing times in practical applications. Therefore it is an aim in this paper to cast the numerical results of the modal analysis into a form which permits fast computations. In the pursuance of this aim the shielding by a building is subdivided into the evaluation of the free field sound pressure of the sound source at the nearest corner and a sequence of single corner scatterings for the evaluation of the sound pressure (incident plus scattered sound) at the next corner. This subdivision is possible under the condition that multiple scattering between succeeding corners can be neglected (i.e., the corners are not too close to each other). The numerical results of the single corner scattering then will be approximated by polynomials which reproduce the analytical results with an error below about 1/2 dB for a cylindrical sound source and about 1/4 dB for an incident plane wave.

The evaluation of noise maps, i.e. of the shielding by buildings, has been described in standard rules and prescriptions, e.g., in reference [3]. The scattering by a building corner there is computed with the well-known Maekawa formula,

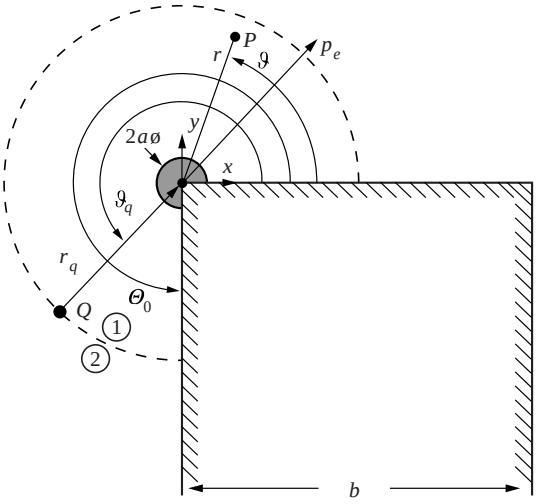

Figure 1. Scheme and co-ordinates of a rigid corner with "wedge angle" Θ_0 and a line source at Q with co-ordinates (r_q, ϑ_q). The radius r_q defines two field zones (1) and (2). See the text for the cylinder with diameter $2a$ at the corner.

i.e., as a function of the ratio s/λ_0 of the difference s of the path length from the line source over the corner to the receiver minus the direct source-receiver distance to the wave length λ_0. The application of the Maekawa formula implicitly assumes that the scattering is produced by a thin screen which, in our notation, is associated with a wedge angle $\Theta_0 = 2\pi$; and it is further assumed that the point of immission is in the far field. It will be seen below that the wedge angle of the building corner (e.g., $\Theta_0 = 3\pi/2$ for a cubic building) is deeply involved in the analysis. It is of some interest to compare results obtained by using the real wedge angle of a corner with those obtained by using the wedge angle of a screen.

The next section is concerned with the single corner scattering for a line source which is parallel to the corner (in Figure 1 the distance b of the second corner is supposed to be very large). In the following section the source radius r_q goes to infinity, leading to the analysis of the single corner scattering for an incident plane wave. Numerical examples will then show that at some distance from the scattering corner the sound field at the flank behind the corner is similar to a field pattern which a line source placed in the corner would produce there. Thus, in the evaluation of the scattering at the next corner, the first corner can be replaced by an equivalent line source. This finding is the basis for the repeated single corner scattering in the determination of the shielding of a building. The final procedure will be the simplification of the sound pressure level computations by polynomials (instead of lengthy sums of Bessel and Hankel functions). These simplifications will be performed for three wedge angles: $\Theta_0 = 270^\circ$, which belongs to the important case of rectangular building corners, and $\Theta_0 = 225^\circ$ which together with $\Theta_0 = 270^\circ$ are the wedge angles at the eaves and the ridge of a typical saddle roof, and $\Theta_0 = 360^\circ$, which belongs to a thin rigid screen. In the last case the usual condition of large kr, kr_q can be avoided here.

2. SINGLE CORNER SCATTERING WITH A LINE SOURCE

For this problem one can take the co-ordinates of Figure 1 (with $b \to \infty$) and a line source at Q with the source co-ordinates r_q, ϑ_q. The source radius r_q defines the zone (1) with $0 \leqslant r \leqslant r_q$ and the zone (2) with $r \geqslant r_q$. Evidently the sound field must be steady at $r = r_q$, except at $\vartheta = \vartheta_q$. The cylinder with diameter $2a$ at the corner in this paper is an artefact (in a forthcoming paper it will play the main part); it is assumed to have a locally reacting surface with a radial surface admittance G (a rigid cylinder with $G = 0$ is just a special case). The introduction of this cylinder takes out the corner apex from the sound field and so avoids discussions in the field formulation's behaviour at the origin. Following this, the cylinder will vanish by the limit procedure $a \to 0$, giving the result without the artefact.

Field formulations of the form

$$p(r, \vartheta, z) = \sum_{\eta} R_\eta(r) T(\eta\vartheta) Z(k_z z) \tag{1}$$

are sought, where the factor $Z(k_z z)$ may be one of the functions $e^{\pm jk_z z}$, $\cos(k_z z)$, $\sin(k_z z)$ or a linear combination thereof with a given wave number k_z. Because $Z(k_z z)$ will appear as a factor in all field representations, one can drop it (like the time factor $e^{j\omega t}$); the only consequence of a value $k_z \neq 0$ will be a modification of the radial wave number (see below). A general form of the azimuthal factor is $T(\eta\vartheta) = a_\eta \cos(\eta\vartheta) + b_\eta \sin(\eta\vartheta)$. With the choice of the ϑ-origin in a rigid flank the second term disappears: i.e., $T(\eta\vartheta) = \cos(\eta\vartheta)$. The terms summed in equation (1) are orthogonal over ϑ in $0 \leqslant \vartheta \leqslant \Theta_0$ if $\eta = \text{const}(\vartheta)$, and they satisfy the boundary conditions at the two rigid flanks if they are solutions of the characteristic equation

$$(\eta_n \Theta_0) \tan(\eta_n \Theta_0) = 0. \tag{2}$$

Solutions of equation (2) are $\eta_n = n\pi/\Theta_0$, $n = 0, 1, 2, \ldots$. Because also $\eta = \text{const}(r)$ holds, the wave equation for the nth mode in the co-ordinates r, ϑ becomes

$$\left(\frac{\partial^2}{\partial r^2} + \frac{1}{r}\frac{\partial}{\partial r} + \frac{1}{r^2}\frac{\partial^2}{\partial \vartheta^2} + k^2\right) p_n(r, \vartheta) = \left(\frac{\partial^2}{\partial r^2} + \frac{1}{r}\frac{\partial}{\partial r} + k^2 - \frac{\eta_n^2}{r^2}\right) p_n(r, \vartheta) = 0,$$

$$k^2 = k_0^2 - k_z^2, \tag{3}$$

which is a Bessel differential equation with general solutions of the form

$$R_\eta(r) = R_n(kr) = c_n \mathrm{H}_{\eta_n}^{(1)}(kr) + d_n \mathrm{H}_{\eta_n}^{(2)}(kr), \tag{4}$$

where $\mathrm{H}_{\eta_n}^{(i)}(kr)$ are Hankel functions, propagating radially inward for $i = 1$ and outward for $i = 2$. They have orders $\eta_n \geqslant 0$ which either are fractional or real in general (depending on the value of Θ_0).

Therefore, one can formulate the sound field in the zone (1) with $a \leqslant r < r_q$ as

$$p_1(r, \vartheta) = \sum_{n \geqslant 0} A_n \mathrm{H}_{\eta_n}^{(2)}(kr_q)[\mathrm{H}_{\eta_n}^{(1)}(kr) + r_n \mathrm{H}_{\eta_n}^{(2)}(kr)] \cos(\eta_n \vartheta),$$

$$Z_0 v_{r1} = \frac{jk}{k_0} \sum_{n \geqslant 0} A_n \mathrm{H}_{\eta_n}^{(2)}(kr_q)[\mathrm{H}_{\eta_n}^{\prime(1)}(kr) + r_n \mathrm{H}_{\eta_n}^{\prime(2)}(kr)] \cos(\eta_n \vartheta), \tag{5}$$

and in zone (2) with $r_q < r < \infty$ as

$$p_2(r, \vartheta) = \sum_{n \geqslant 0} A_n [\mathrm{H}_{\eta_n}^{(1)}(kr_q) + r_n \mathrm{H}_{\eta_n}^{(2)}(kr_q)] \mathrm{H}_{\eta_n}^{(2)}(kr) \cos(\eta_n \vartheta),$$

$$Z_0 v_{r2} = \frac{jk}{k_0} \sum_{n \geqslant 0} A_n [\mathrm{H}_{\eta_n}^{(1)}(kr_q) + r_n \mathrm{H}_{\eta_n}^{(2)}(kr_q)] \mathrm{H}_{\eta_n}^{\prime(2)}(kr) \cos(\eta_n \vartheta). \tag{6}$$

A prime on the functions indicates the derivative with respect to the argument. This formulation satisfies the boundary conditions at the flanks and Sommerfeld's

far field condition; it is steady in the sound pressure at the zone limit $r = r_q$. It contains inward and outward propagating modes for $r < r_q$ and only outward propagating modes in $r > r_q$. The factors r_n evidently are radial reflection factors; they can be defined at the surface of the cylinder covering the origin. Due to the orthogonality of the modes, the boundary condition at the cylinder must be obeyed term-wise, giving

$$r_n = -\frac{Z_0 G \mathrm{H}^{(1)}_{\eta_n}(ka) + \mathrm{j}(k/k_0)\mathrm{H}'^{(1)}_{\eta_n}(ka)}{Z_0 G \mathrm{H}^{(2)}_{\eta_n}(ka) + \mathrm{j}(k/k_0)\mathrm{H}'^{(2)}_{\eta_n}(ka)}$$

$$= -\frac{[(\eta_n/k_0 a) - \mathrm{j}Z_0 G]\mathrm{H}^{(1)}_{\eta_n}(ka) - (k/k_0)\mathrm{H}^{(1)}_{\eta_n+1}(ka)}{[(\eta_n/k_0 a) - \mathrm{j}Z_0 G]\mathrm{H}^{(2)}_{\eta_n}(ka) - (k/k_0)\mathrm{H}^{(2)}_{\eta_n+1}(ka)}. \tag{7}$$

In the second line the known relation for derivatives of Hankel functions was used. In the limit $a \to 0$, neglecting Bessel functions as compared to Neumann functions, which both are contained in the Hankel functions $\mathrm{H}^{(1,2)}_\nu(ka) = \mathrm{J}_\nu(ka) \pm \mathrm{j}\mathrm{Y}_\nu(ka)$, one gets $r_n \to 1$ for $a \to 0$. In that limit the field formulations become

$$p_1(r, \vartheta) = 2 \sum_{n \geqslant 0} A_n \mathrm{H}^{(2)}_{\eta_n}(kr_q)\mathrm{J}_{\eta_n}(kr) \cos(\eta_n \vartheta),$$

$$p_2(r, \vartheta) = 2 \sum_{n \geqslant 0} A_n \mathrm{J}_{\eta_n}(kr_q)\mathrm{H}^{(2)}_{\eta_n}(kr) \cos(\eta_n \vartheta). \tag{8}$$

One boundary condition is still available: the fitting of the radial particle velocities at the zone limit $r = r_q$ to the volume flow of the line source, i.e., the relation

$$v_{r2}(r_q + 0) - v_{r1}(r_q - 0) \stackrel{!}{=} q\delta(\vartheta - \vartheta_q), \tag{9}$$

where q is the volume flow density of the source and $\delta(\vartheta - \vartheta_q)$ is the Dirac function. The sound pressure field of the line source (the factor $Z(k_z z)$, which is "produced" by the source, is dropped here also) in the radial co-ordinate ρ centred at the source is

$$p_Q(\rho) = \tfrac{1}{4} Z_0 k_0 \rho q \mathrm{H}^{(2)}_0(k\rho). \tag{10a}$$

In fact this relation can be used to express q by the free field sound pressure $p_Q(\rho)$ at a distance ρ:

$$Z_0 q = \frac{4}{k_0 \rho \mathrm{H}^{(2)}_0(k\rho)} p_Q(\rho). \tag{10b}$$

Because $\cos(\eta_n \vartheta)$ is a complete orthogonal set of functions, one can expand the Dirac function in such terms:

$$\delta(\vartheta - \vartheta_q) = \sum_{n \geqslant 0} b_n \cos(\eta_n \vartheta). \tag{11}$$

Application of the integral

$$\int_0^{\Theta_0} \cdots \cos(\eta_n \vartheta)\, \mathrm{d}\vartheta$$

to both sides gives on the left-hand side $\cos(\eta_n \vartheta_q)$ and on the right-hand side $\Theta_0 N_n b_n$ with the norms N_n of the modes given by

$$N_n = \frac{1}{\Theta_0}\int_0^{\Theta_0} \cos^2(\eta_n \vartheta)\, \mathrm{d}\vartheta = \frac{1}{2}\left(1 + \frac{\sin(2\eta_n \Theta_0)}{2\eta_n \Theta_0}\right) = \begin{Bmatrix} 1, & n = 0 \\ 1/2, & n > 0 \end{Bmatrix}. \tag{12}$$

Thus:

$$\delta(\vartheta - \vartheta_q) = \frac{1}{\Theta_0}\sum_{n \geqslant 0} \frac{1}{N_n} \cos(\eta_n \vartheta_q)\cos(\eta_n \vartheta). \tag{13}$$

The boundary condition (9) must be satisfied term-wise (again because of the orthogonality of the modes), which leads to

$$A_n[\mathrm{H}_{\eta_n}^{(1)}(kr_q)\mathrm{H}_{\eta_n}'^{(2)}(kr_q) - \mathrm{H}_{\eta_n}'^{(1)}(kr_q)\mathrm{H}_{\eta_n}^{(2)}(kr_q)] = -\mathrm{j}\frac{k_0}{k}\frac{Z_0 q}{\Theta_0 N_n}\cos(\eta_n \vartheta_q). \tag{14}$$

The bracket contains the Wronski determinant of Hankel functions with the value $[\cdots] = -4\mathrm{j}/(\pi k r_q)$, and one has

$$A_n = \frac{\pi}{4} k_0 r_q \frac{Z_0 q}{\Theta_0 N_n}\cos(\eta_n \vartheta_q) = \frac{\pi}{\Theta_0 N_n}\frac{p_Q(0)}{\mathrm{H}_0^{(2)}(kr_q)}\cos(\eta_n \vartheta_q). \tag{15}$$

In this last expression equation (10b) has been used in which the free field sound pressure of the source at the corner is denoted by $p_Q(0)$, because the corner is the origin of the co-ordinate system (r, ϑ). Thus, the sound pressure field around a single rigid corner, which is excited by a line source producing a free field sound pressure $p_Q(0)$ at the corner, is known from equations (15) and (8).

The limit $r_n \to 1$ for $a \to 0$ in equation (7) is difficult to show analytically. This is one reason for applying the identical replacement

$$r_n = 1 + (r_n - 1) = 1 - 2C_n, \qquad 2C_n = 1 - r_n, \tag{16}$$

to get

$$C_n = \frac{Z_0 G \mathrm{J}_{\eta_n}(ka) + \mathrm{j}(k/k_0)\mathrm{J}_{\eta_n}'(ka)}{Z_0 G \mathrm{H}_{\eta_n}^{(2)}(ka) + \mathrm{j}(k/k_0)\mathrm{H}_{\eta_n}'^{(2)}(ka)},$$

$$C_n \xrightarrow[Z_0 G \to 0]{} \frac{\mathrm{J}_{\eta_n}'(ka)}{\mathrm{H}_{\eta_n}'^{(2)}(ka)}, \qquad C_n \xrightarrow[Z_0 G \to \infty]{} \frac{\mathrm{J}_{\eta_n}(ka)}{\mathrm{H}_{\eta_n}^{(2)}(ka)}, \qquad C_n \xrightarrow[ka \to 0]{} 0. \tag{17}$$

With this replacement the field formulations for a corner with a cylinder around the origin become

$$p_1(r, \vartheta) = p_{1,Corner} + p_{1,Cyl}$$

$$= \frac{2\pi}{\Theta_0} \frac{p_Q(0)}{\mathrm{H}_0^{(2)}(kr_q)} \sum_{n \geqslant 0} \frac{\cos(\eta_n \vartheta_q)}{N_n} \mathrm{H}_{\eta_n}^{(2)}(kr_q) \mathrm{J}_{\eta_n}(kr) \cos(\eta_n \vartheta)$$

$$- \frac{2\pi}{\Theta_0} \frac{p_Q(0)}{\mathrm{H}_0^{(2)}(kr_q)} \sum_{n \geqslant 0} C_n \frac{\cos(\eta_n \vartheta_q)}{N_n} \mathrm{H}_{\eta_n}^{(2)}(kr_q) \mathrm{H}_{\eta_n}^{(2)}(kr) \cos(\eta_n \vartheta), \tag{18a}$$

$$p_2(r, \vartheta) = p_{2,Corner} + p_{2,Cyl}$$

$$= \frac{2\pi}{\Theta_0} \frac{p_Q(0)}{\mathrm{H}_0^{(2)}(kr_q)} \sum_{n \geqslant 0} \frac{\cos(\eta_n \vartheta_q)}{N_n} \mathrm{J}_{\eta_n}(kr_q) \mathrm{H}_{\eta_n}^{(2)}(kr) \cos(\eta_n \vartheta)$$

$$- \frac{2\pi}{\Theta_0} \frac{p_Q(0)}{\mathrm{H}_0^{(2)}(kr_q)} \sum_{n \geqslant 0} C_n \frac{\cos(\eta_n \vartheta_q)}{N_n} \mathrm{H}_{\eta_n}^{(2)}(kr_q) \mathrm{H}_{\eta_n}^{(2)}(kr) \cos(\eta_n \vartheta). \tag{18b}$$

The sound fields in the two zones are split into two sums. The first sum does not contain any information about the cylinder, and for $C_n \to 0$ if $a \to 0$ it becomes the field formulation of equations (8); so it represents the field of the corner without the cylinder. The second sum represents the field contribution due to the existence of the cylinder. It will be the topic of a forthcoming paper to describe the potential for improving the sound shielding of corners if they are equipped with cylinders of a "suitable" surface admittance, and how a suitable admittance can be defined and realised. A similar analysis was used by Möser [4], and at the same time by this author [5], to evaluate the efficiency of absorbing cylinders on screens to improve the shielding; the wedge angle in the case of a screen is $\Theta_0 = 2\pi$, and $\eta_n = n/2$.

3. SINGLE CORNER SCATTERING WITH AN INCIDENT PLANE WAVE

The plane wave incidence case is obtained by displacing the line source to infinity, $r_q \to \infty$, letting $\vartheta_q = \text{const}$ and increasing the volume flow density q of the source so that the free field sound pressure $p_Q(0)$ at the corner remains the same. Using the asymptotic expansion of Hankel functions one gets

$$\frac{\mathrm{H}_{\eta_n}^{(2)}(kr_q)}{\mathrm{H}_0^{(2)}(kr_q)} \xrightarrow[r_q \to \infty]{} \mathrm{e}^{\mathrm{j}\eta_n \pi/2} \tag{19}$$

and with this from equation (18a) (now all the field is in zone (1)) becomes

$$p(r, \vartheta) = p_{Corner} + p_{Cyl}$$

$$= \frac{2\pi}{\Theta_0} p_Q(0) \sum_{n \geqslant 0} \frac{e^{j\eta_n \pi/2}}{N_n} J_{\eta_n}(kr) \cos(\eta_n \vartheta_q) \cos(\eta_n \vartheta)$$

$$- \frac{2\pi}{\Theta_0} p_Q(0) \sum_{n \geqslant 0} C_n \frac{e^{j\eta_n \pi/2}}{N_n} H^{(2)}_{\eta_n}(kr) \cos(\eta_n \vartheta_q) \cos(\eta_n \vartheta). \tag{20}$$

Again the second sum disappears if there is no cylinder at the origin. Note that the first sum can be reduced to the Fresnel integral in the case of $\Theta_0 = 2\pi$, and the Fresnel integral is a part of the sum for Θ_0 being a small fraction of π; but since such simplifications are not possible for general values of Θ_0 this possibility is not displayed here in more detail.

4. NUMERICAL EVALUATION METHODS

Henceforth only the first sums in equations (18a), (18b) and (20) are considered. These expressions are simple in their structure, but possibly their numerical evaluation is delicate. The critical question is "up to which index limit n_{hi} should the summation proceed?" The answer is relatively easy in the case of equation (20). There the convergence of the sum is produced by the Bessel functions $J_{\eta_n}(kr)$. These functions steeply decrease with increasing n, if $\eta_n > kr$. If the summation is performed until the Bessel functions have assumed an order of magnitude $|J_{\eta_n}(kr)| \approx 10^{-M}$, with $M = 8$ as a reasonable compromise between precision and computing time, then the summation should proceed up to

$$n_{hi} \approx \frac{\Theta_0}{\pi} \left\{ 1 + kr \left[1 + 1{\cdot}915 \left(\frac{M-1}{kr} \right)^{0{\cdot}676} \right] \right\}. \tag{21}$$

kr will be allowed to go up to $kr = 100$; the n_{hi} then assume values of about $n_{hi} = 200$ for $\Theta_0 = 3\pi/2$.

The evaluation becomes delicate in the case of a line source, i.e., of the equations (18a) and (18b). There the Bessel function contains as argument the smaller one of the two values kr, kr_q, and the Hankel function has the larger value as its argument. When the order η_n of the Neumann function $Y_{\eta_n}(x)$ (which is contained in the Hankel function) exceeds the argument x, then the Neumann function steeply increases. Even then the sums would converge if the functions in the terms were computed with a very high precision, but the convergence then is produced by a partial compensation of large terms with alternating signs. It is known that this principle of convergence fails if the terms are evaluated with numerical errors. The sums in equations (18a) and (18b) then assume the behaviour of asymptotic sums: they converge up to a certain limit of the summation index; if this limit is exceeded they diverge. Therefore, the summations in equations (18a) and (18b) are performed without a convergence test up to an index n_{hi} which is obtained from

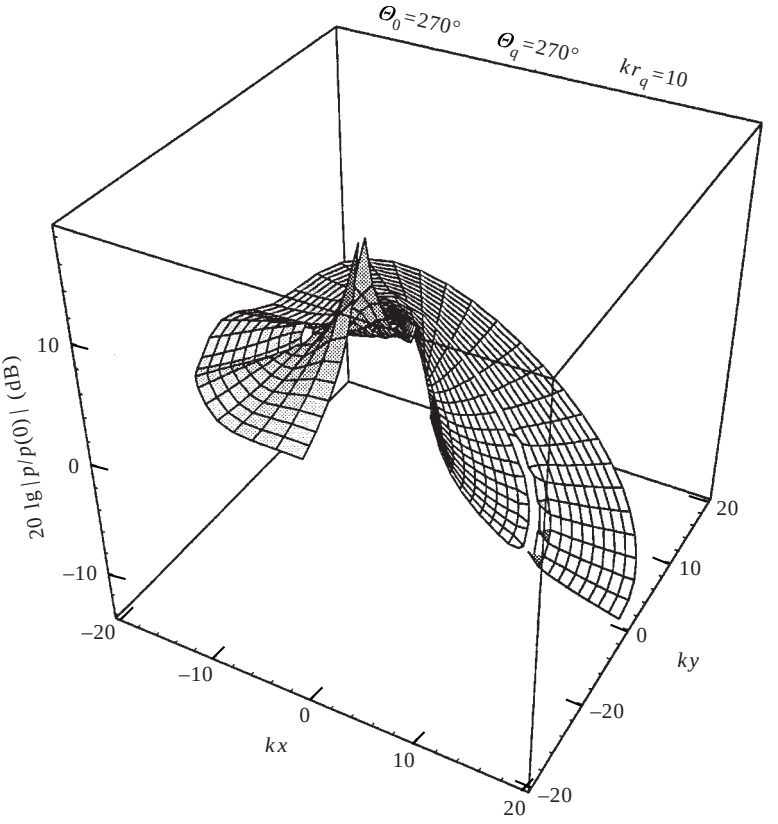

Figure 2. Sound pressure level around a right-angled rigid corner produced by a line source at (r_q, ϑ_q) on the illuminated flank. The ring-shaped gap is at $kr = kr_q$.

equation (21) by setting $M = 4$. The summation then is continued as long as the relative contribution |term|/|sum| of a new term is smaller than the contribution of the earlier term. The most critical situation evidently is the case $kr = kr_q$. With an eight-digit precision in the evaluation of the Hankel functions the errors become visible in the final sound pressure levels at $kr = kr_q$ with deviations of about ± 1 dB for small kr values, increasing up to about $\pm 2{\cdot}5$ dB at $kr = 100$ if $kr = kr_q$ is avoided. These errors shall be tolerated, because the final acquisition of the results (representation of the levels by polynomials) will eliminate these errors (see below).

In any case, however, the computing time with the analytical expressions for the sound pressure field is prohibitively long in practical tasks where a great number of sound pressure level computations must be performed (where computing times are indicated below, they are those for evaluations with non-compiled Mathematica® programs on a 35-MHz computer; compiled programs on modern computers would be much faster). That is the reason for recasting the results in a more easily computable form, which will be described in a later section.

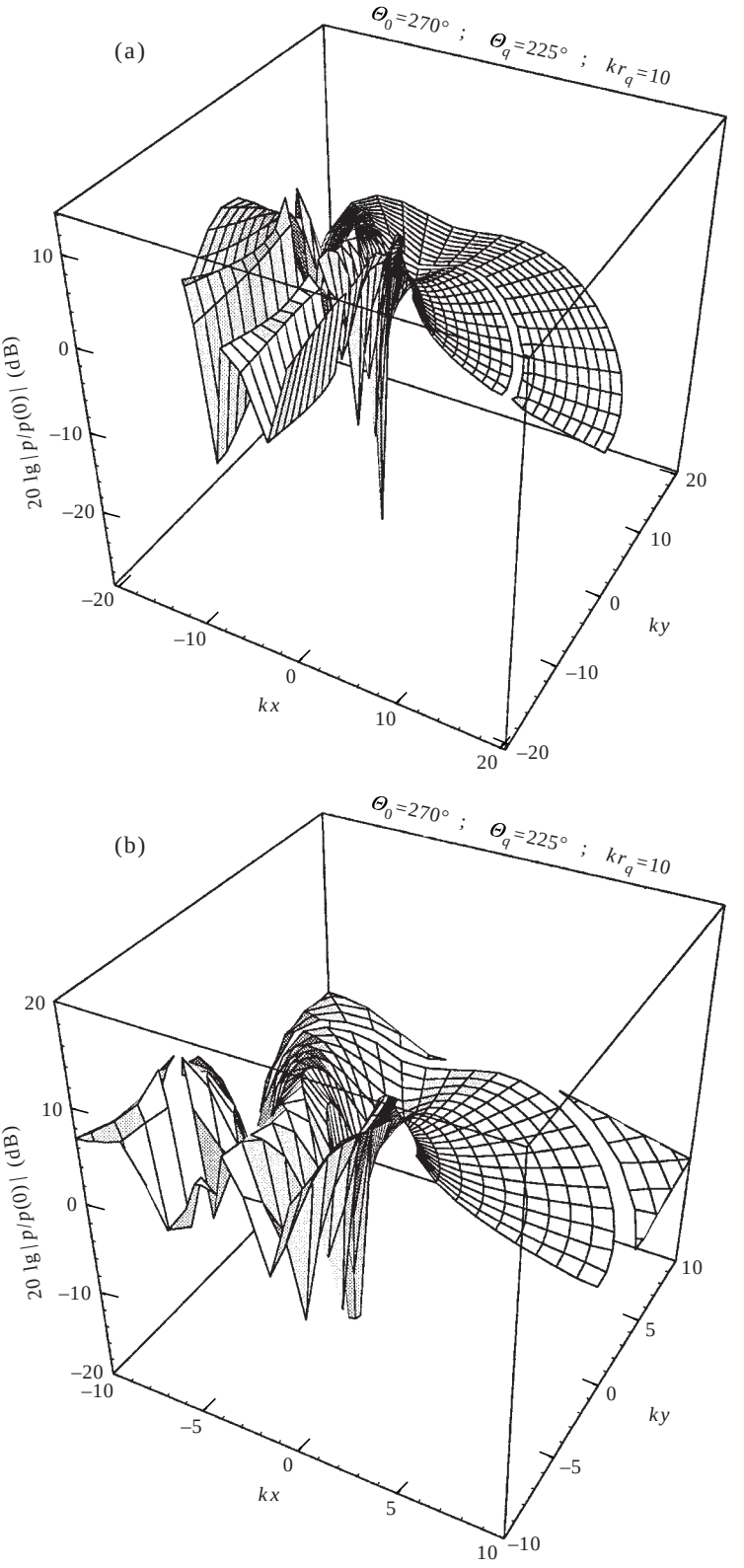

Figure 3—(*Caption opposite*).

5. NUMERICAL RESULTS OF SINGLE CORNER SCATTERING WITH A LINE SOURCE

In this section the corner is mostly right-angled, i.e., the wedge angle is $\Theta_0 = 3\pi/2$ or 270°. A line source is considered first. The sound pressure distribution of the factor $Z(k_z z)$ along the corner direction must not be discussed, because the sound pressure field $p(kr, \vartheta)$ is referred to the sound pressure $p_Q(0)$ of the source at the corner, which would have the same factor, so that the common factor would cancel. And the modification of the radial wave number from k_0 to k according to equation (3) must not be considered if one uses kr and kr_q as radial variables.

Figure 2 shows a 3D-plot of the sound pressure level $L(kr, \vartheta) = 20 \lg |p(kr, \vartheta)/p_Q(0)|$ for $kr_q = 10$ and $\Theta_0 = \vartheta_q = 270^\circ$ (i.e., the line source is on the "illuminated" flank); the radial variable is changing in steps of $\Delta kr = 1$ (beginning with $kr_{min} = 0{\cdot}5$) and the angle ϑ of the field point in steps $\Delta\vartheta = 7{\cdot}5^\circ$. The gap in the radial direction indicates $kr = kr_q$. The peak is at the place of the source; the level there is finite, because $kr = kr_q$ is avoided (the evaluation of the graph takes about 8 min). Figure 3(a) is a similar diagram, only the source angle is changed to $\vartheta_q = 225^\circ$; Figure 3(b) with the same parameters shows more details in zone (1) with $kr < kr_q$. The interference variations on the illuminated side are much stronger if the source is a distance from the flank rather than with the source on the flank. The field in the shadow zone, however, is steady. It is important to note that the field approaches the shadow flank with a zero slope. Thus, the field pattern at the shadow flank in the azimuthal direction is very similar to the pattern which a line source in the corner with a suitable source strength would produce at this flank. This finding is the basis for the procedure of the field evaluation behind more than one corner, which will be described below; the field at a succeeding corner is assumed as being produced by a line source in the preceding corner.

For that procedure one needs the sound pressure level on the shadow flank, i.e., for $\vartheta = 0$. Figure 4(a) shows $L(kr, 0)$ over kr for a small source distance $kr_q = 3{\cdot}55$, and Figure 4(b) shows this for a larger source distance $kr_q = 56{\cdot}6$ (the values of kr_q were selected midway between sampling points of kr); in both diagrams the source angle ϑ_q is varied. In Figure 4(a) variations of the curves can be seen at $kr \approx kr_q$ due to numerical errors (as explained in the previous section). These variations disappeared when the computation was repeated with a 15-digit precision of the Hankel functions; thus they can be ignored in the further discussions. The branch of the curves for $kr > kr_q$ is a smooth continuation of the branch for $kr < kr_q$, although both branches are generated by different equations, (18b) and (18a), respectively. The parameter values of ϑ_q in Figures 4(a) and 4(b) begin with $\vartheta_q = 180^\circ$, for which the second flank changes from a flank in the shadow to a directly illuminated flank. The influence of kr_q is greatest near to this transition condition. At high kr values the curves tend to a slope like $1/\sqrt{kr}$. This can be used for the extension of the range of kr beyond the value $kr = 100$, which

Figure 3. (a) Sound pressure level around a right-angled rigid corner produced by a line source at (r_q, ϑ_q) at a distance from the illuminated flank. (b) As (a) but with a reduced range $kr \leqslant kr_q$, to show more details.

was the limit imposed by numerical errors (the value $10 \lg (100/kr)$ is added to $L(100, 0)$).

The next diagrams are concerned with the comparison of the corner scattering with the screen scattering. Figures 5(a, b) show $L(kr, 0)$ over kr for source distances $kr_q = 3{\cdot}55$ and $kr_q = 56{\cdot}6$, respectively, for a variable corner angle Θ_0 and with $\vartheta_q = \Theta_0$ (i.e., both the source and the receiving point are on flanks). As could have been expected, the level reduction is strongest for a screen. In these diagrams

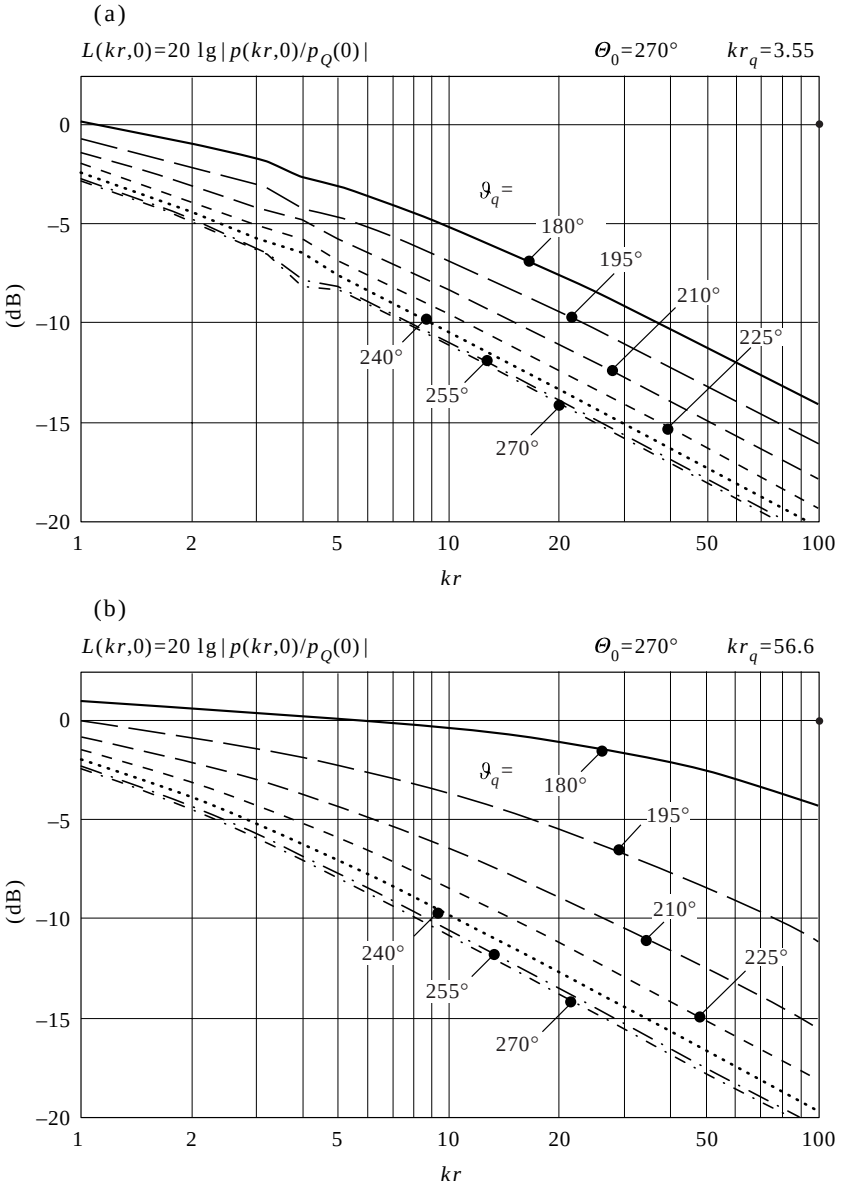

Figure 4. (a) Sound pressure level $L(kr, 0)$ on the shadow flank of a right-angled corner for a line source at the distance $kr_q = 3{\cdot}55$ with different source angles ϑ_q. (b) As (a) but with a larger source distance $kr_q = 3{\cdot}55$.

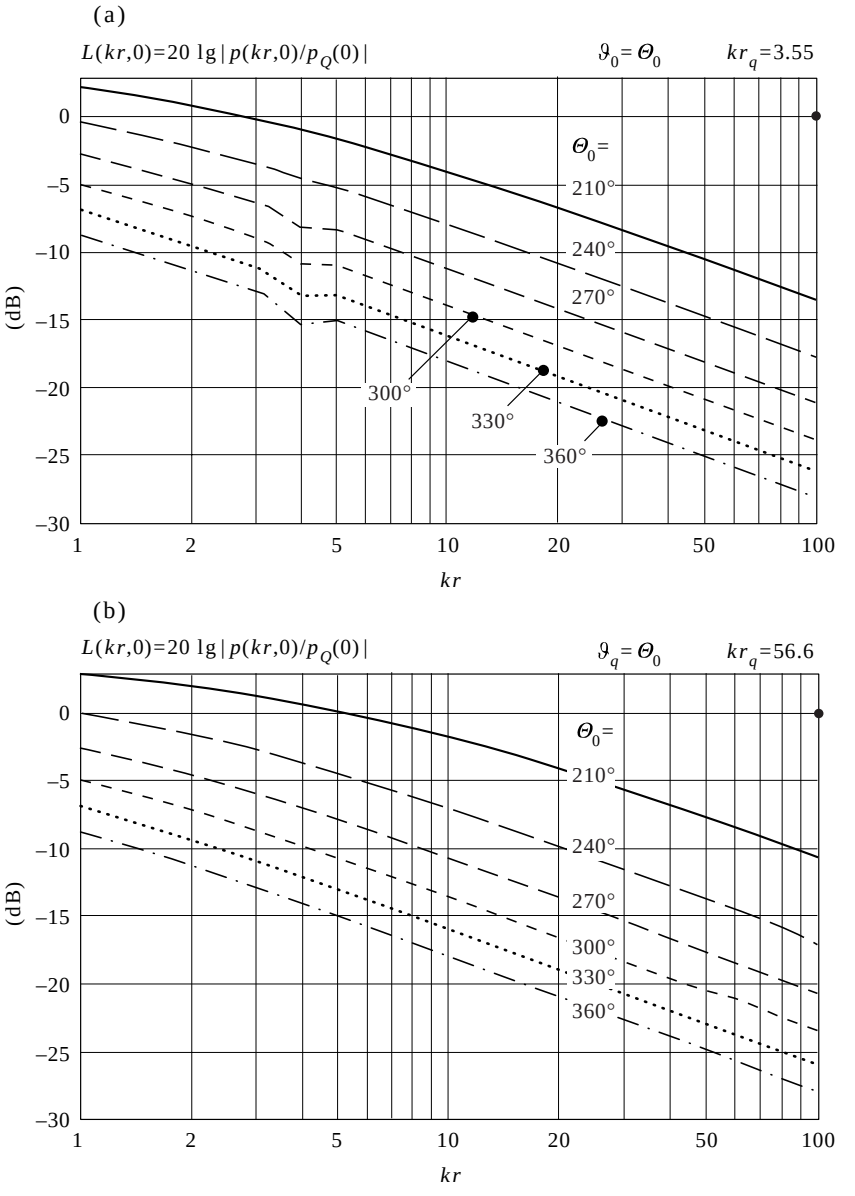

Figure 5. (a) Sound pressure level $L(kr, 0)$ on the shadow flank of corners with different wedge angles Θ_0 for a line source at the distance $kr_q = 3{\cdot}55$ on the illuminated flank; $\vartheta_q = \Theta_0$. (b) As (a) but for a larger source distance $kr_q = 56{\cdot}6$.

the detour $s = (Q, O, P) - (Q, P)$ and the ratio s/λ_0 are the same for all curves with the same value of kr. Evidently the parameter s/λ_0 is not sufficient to describe the scattering at corners with different corner angles. Figures 6(a, b) are similar to Figures 5(a, b) except that now $\vartheta_q = 210^\circ$ is kept constant. Therefore, not only s is constant, but also the deflection angle of the rays (source(Q) − origin(O) − field point(P)). The difference in the level reduction by different corner angles now is smaller than in Figures 5(a, b), but the difference of about $\Delta L \approx 2{\cdot}5$ dB for

$\Theta_0 = 270^\circ$ (right-angled corner) and $\Theta_0 = 360^\circ$ (screen) is estimated as being too high to be simply neglected.

The graphs of Figures 4(a)–6(b) contain $L(kr, 0)$: i.e., the receiving point is on the flank, the source angle ϑ_q is varied. The terms in the sums of equations (18a) and (18b) are insensitive to the exchange $\vartheta \leftrightarrow \vartheta_q$: i.e., to the exchange of receiver angle and source angle. If one exchanges receiver $\leftrightarrow$ source, then (18a) $\leftrightarrow$ (18b) must be exchanged also, if $kr \neq kr_q$. This however needs no special consideration,

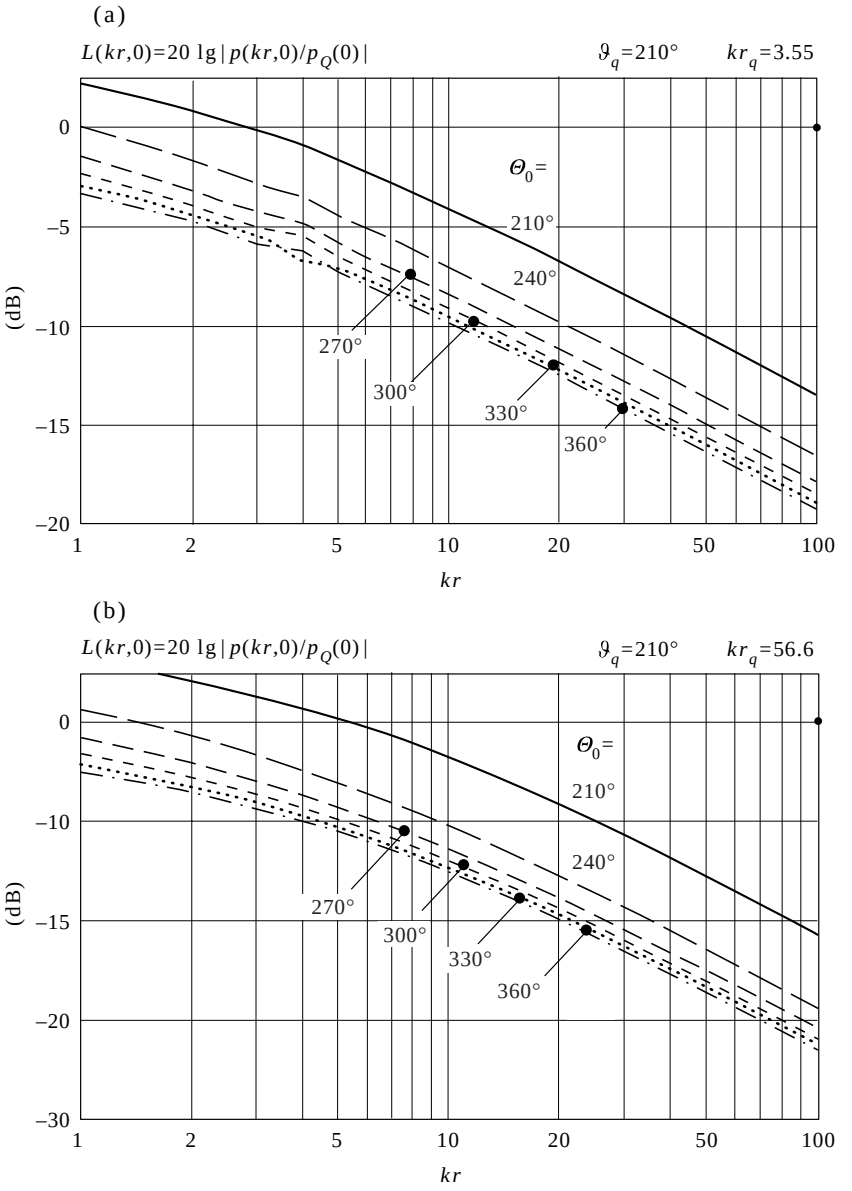

Figure 6. (a) Sound pressure level $L(kr, 0)$ on the shadow flank of corners with different wedge angles Θ_0 for a line source at the distance $kr_q = 3{\cdot}55$ with a fixed source angle $\vartheta_q = 210^\circ$. (b) As (a) but with a larger source distance $kr_q = 56{\cdot}6$.

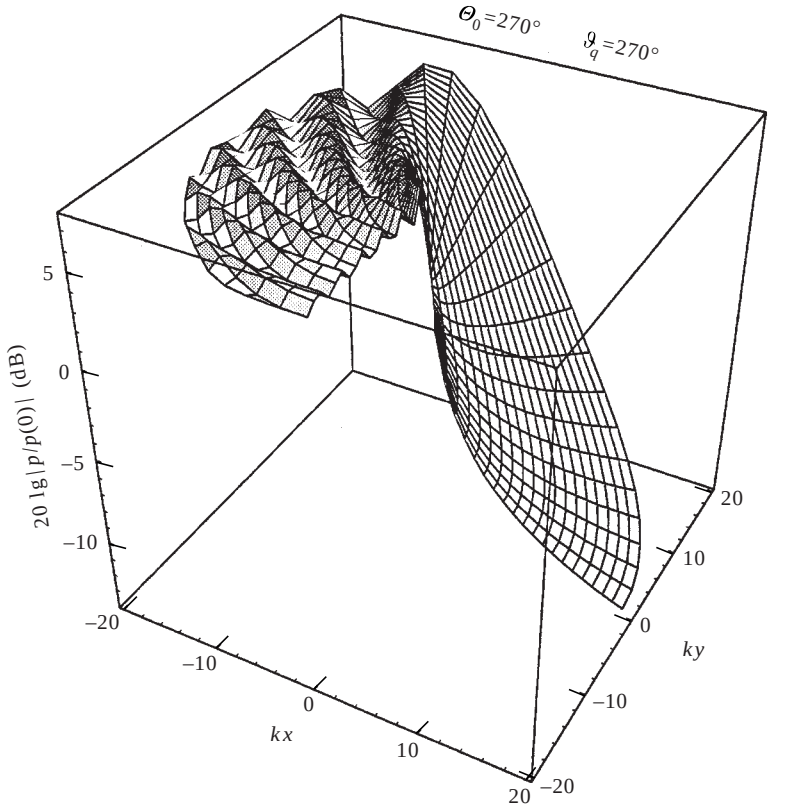

Figure 7. Sound pressure level around a right-angled rigid corner produced by a plane wave from the direction ϑ_q parallel to the illuminated flank.

because the curve branches for the two ranges are continuations of each other. Also the factor $p_Q(0)/H_0^{(2)}(kr_q)$ in front of the sums remains constant if the line source remains the same; the resulting sound pressure which belongs to $L(kr, 0)$ must be corrected with a factor $H_0^{(2)}(kr_q)/H_0^{(2)}(kr)$ after an exchange of source and receiver positions if $p_Q(0)$ is kept constant. Thus, the graphs can be used also for the cases when the source is on the illuminated flank and the receiver is distant of the shadow flank. This fact will save computations in the determination of the sound shielding by buildings (see below).

6. NUMERICAL RESULTS OF SINGLE CORNER SCATTERING WITH AN INCIDENT PLANE WAVE

The above discussion concerning the exchange of receiver and source can now be continued. This exchange now is completely described by the exchange $\vartheta \leftrightarrow \vartheta_Q$, which has no influence on equation (20). Figure 7 contains a 3D-plot of the sound pressure level $L(kr, \vartheta) = 20 \lg |p(kr, \vartheta)/p_Q(0)|$ for $\Theta_0 = \vartheta_q = 270°$ (i.e., the plane wave propagates parallel to the "illuminated" flank); the radial variable is changing in steps of $\Delta kr = 1$ (beginning with $kr_{min} = 0{\cdot}5$) and the angle ϑ of the field point in steps $\Delta\vartheta = 7{\cdot}5°$. Along the illuminated flank there exists a standing

wave pattern coming from the reflection at the corner. The sound pressure level steeply decreases in the shadow zone. In the next 3D-plot of Figure 8 the angle from which the plane wave comes is reduced to $\vartheta_q = 225°$. In front of the illuminated flank there exists a standing wave pattern similar to that which would be produced by the reflection at an infinite rigid wall. However, there are distortions of that pattern (as can be seen at the strong variations of the minima) caused by the scattered wave from the corner. The slope of the level in the shadow zone is smaller than in Figure 7. The last of the 3D-plots, Figure 9, is for a plane wave angle $\vartheta_q = 180°$: i.e., for a propagation parallel to the second flank (the range of kr is reduced). The standing wave pattern on the illuminated side becomes simple only at large distances kr from the corner. On the second flank the sound pressure level becomes constant at larger distances, after a steep slope within a short distance of the corner.

Figure 10 for plane wave incidence corresponds to Figures 4(a, b) for excitation by a line source; the angles ϑ_q are the same for these diagrams. Except for values of $\vartheta_q \approx 180°$ the sound pressure level $L(kr, 0)$ on the shadow flank in Figure 10 with a plane wave agrees quite well with that in Figure 4(b) with a distant line source. In Figure 11 $L(kr, 0)$ is plotted for different wedge and wave angles $\Theta_0 = \vartheta_q$ with a plane wave propagating parallel to the first flank (similar to Figures 5(a, b),

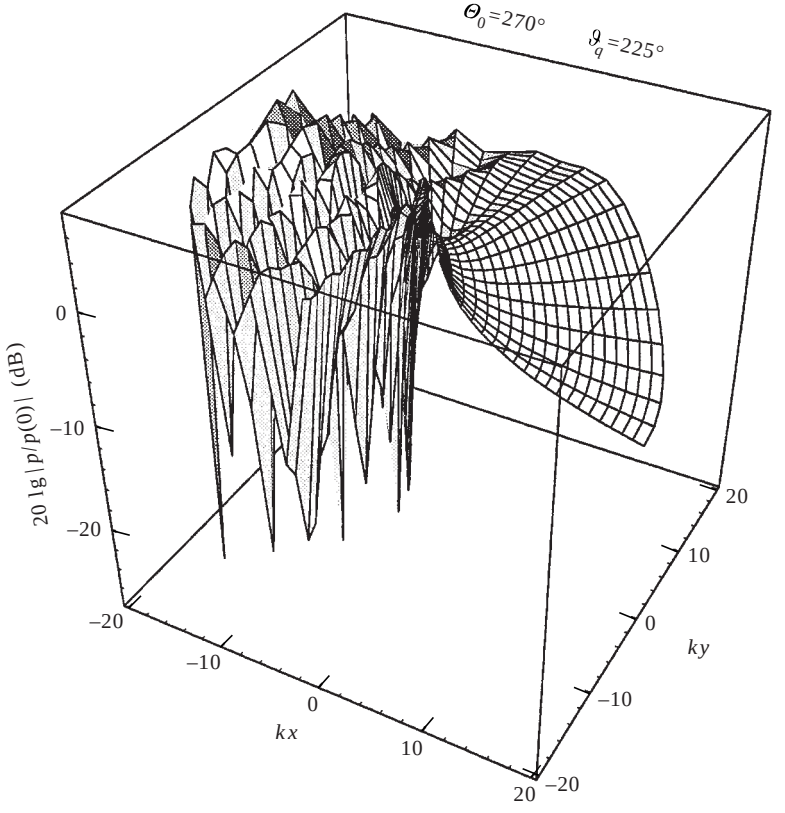

Figure 8. Sound pressure level around a right-angled rigid corner produced by a plane wave from the direction $\vartheta_q = 225°$.

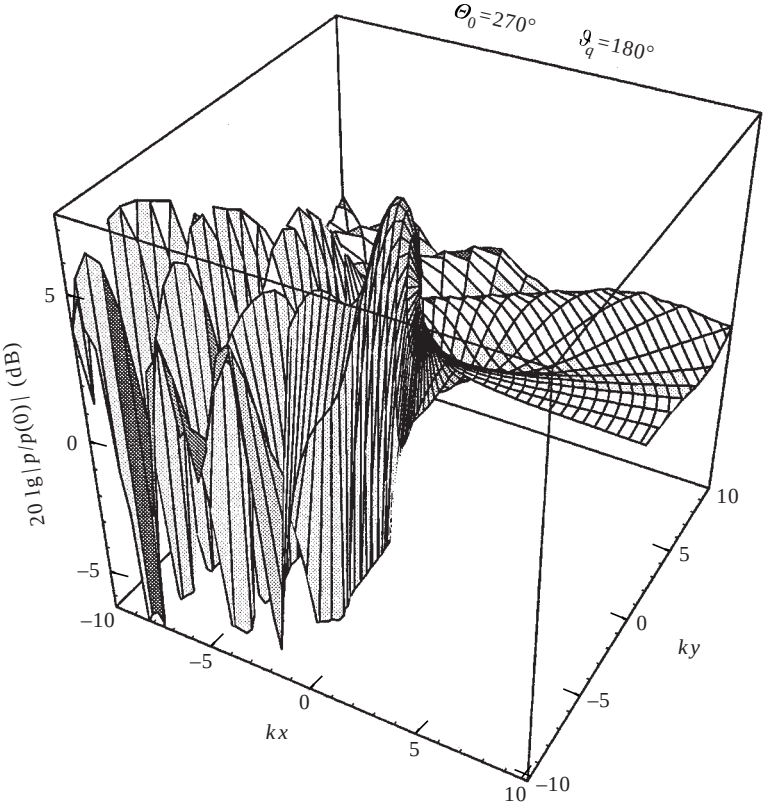

Figure 9. Sound pressure level around a right-angled rigid corner produced by a plane wave from the direction $\vartheta_q = 180°$ parallel to the second flank.

but there with a cylindrical wave). These levels represent the minimum values obtainable by a single corner scattering. The agreement between Figure 5(b) for a distant line source and Figure 11 for a plane wave again is good. Finally Figure 12 represents $L(kr, 0)$ for a constant wave angle $\vartheta_q = 210°$ and different wedge angles Θ_0. It is similar to Figure 6(b), which was for a distant line source. The differences in $L(kr, 0)$ for a plane wave remain below about 2 dB for $270° \leqslant \Theta_0 \leqslant 360°$.

One can now come to the procedure for the determination of the sound shielding by a building, but must discuss first the question of effective sources.

7. EFFECTIVE SOUND SOURCES

The theory as displayed above deals either with a single line source or with a single incident plane wave. The first flank is assumed to extend to infinity. This would correspond to a line source or a plane wave over a totally absorbing ground. We should remember that we need the free field sound pressure level $p_Q(0)$ of the source at the first corner (or more precisely: its absolute magnitude or sound pressure level defined relatively to any reference level).

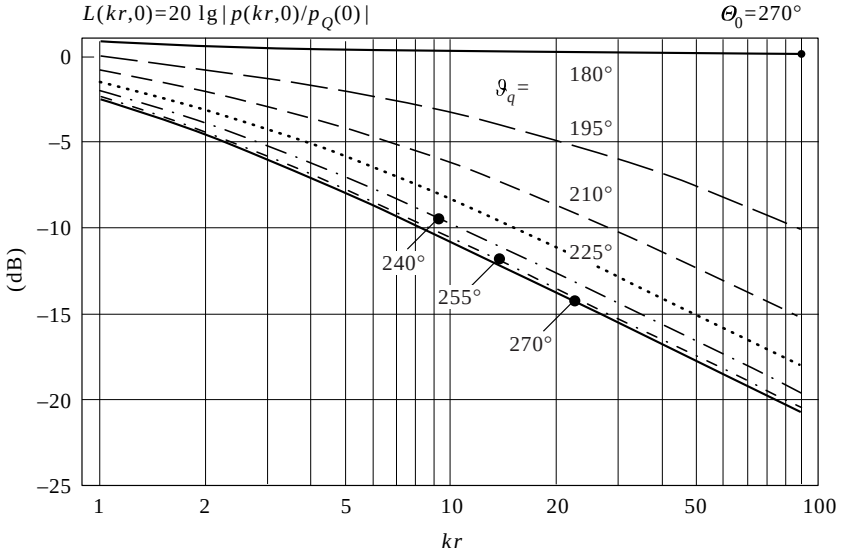

Figure 10. Sound pressure level $L(kr, 0)$ on the shadow flank of a right-angled corner for a plane wave with different source angles ϑ_q.

Usually traffic noise is described as coming from an effective line source. If the traffic noise level is acquired by measurements, then the ground reflection is already included in the source strength and must not be considered separately. If the noise comes from an elevated railway or from an overhead street, then the computation should be repeated for the original source and for a source which is mirror-reflected at the ground. Any ground absorption can be introduced by a suitable reflection coefficient of the ground as a strength factor of the mirror

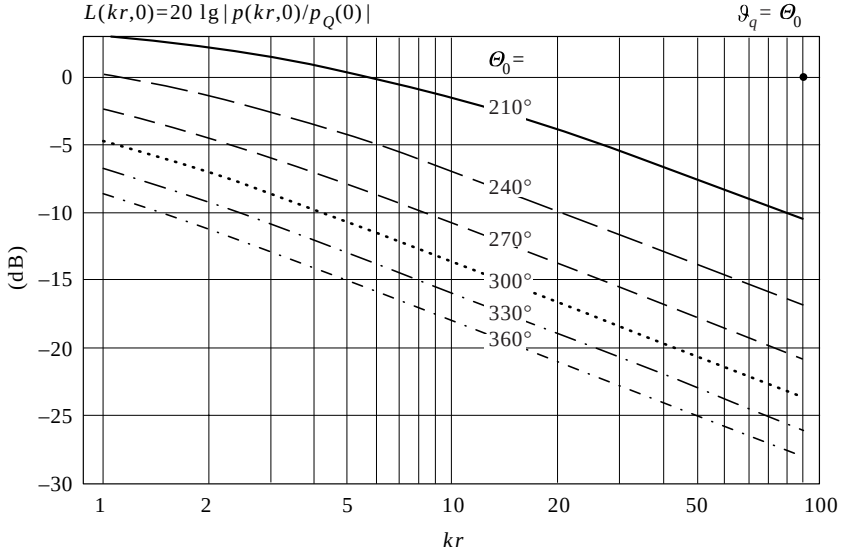

Figure 11. Sound pressure level at the second flank of corners with different wedge angle Θ_0 for a plane wave incident parallel to the first flank.

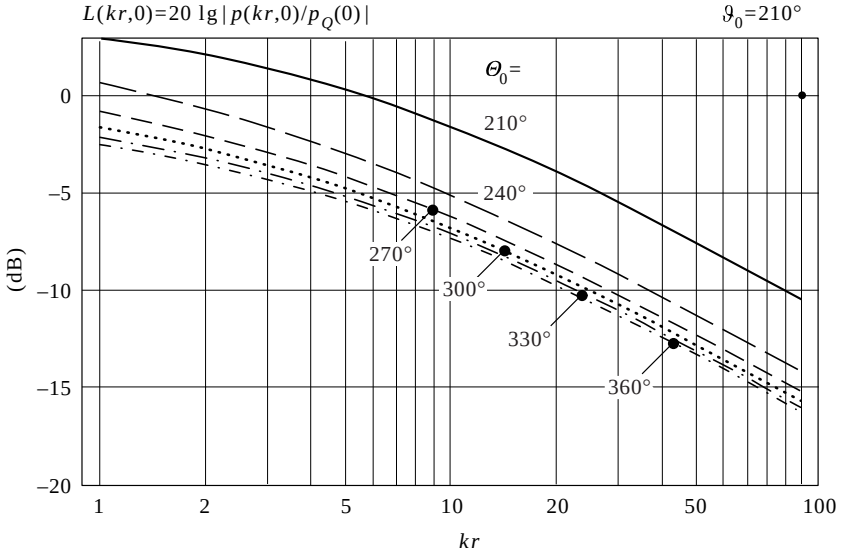

Figure 12. Sound pressure level at the second flank of corners with different wedge angle Θ_0 for a plane wave incident with a fixed source angle $\vartheta_q = 210°$.

source. Because the sound signals from the original source and from the mirror source become incoherent for sufficiently large distances between the two sources, the squared magnitudes of the final sound pressure from the repeated calculations can be added. For more precise calculations with coherent original and mirror-reflected source, i.e., for smaller distances between them, the complex results of the repeated calculations should be added (then, however, the condensed form of the sound pressure level computation described below is no longer applicable, and the analytical field representations from above should be used). If the distance between the original and the reflected source is small, then it is better and easier to start with an effective single source, especially if its distance to the first corner is large enough.

A plane wave may be used as a representation for a sufficiently far away source. A separate consideration of the original plane wave and of its ground reflection generally will be necessary for elevated sources only. Most of the results shown above are for sources which are below the prolongation of the second flank (i.e., which lie below the horizon of the corner as seen from the receiving point). The results indicate that it generally does not pay (in the present context of noise shielding) to apply a scattering calculation to a corner the second flank of which is directly illuminated. When the "first corner" is mentioned in what follows, then it is the first corner for which the source is below the horizon.

The present calculations and results also can be applied approximately for point sources in the plane containing the source and normal to the corner, if $kr_q \gg 1$ so that the spherical variation of the field along the corner becomes small. Then a line source with $k_z = 0$ in the source position would be a suitable model.

8. CALCULATION OF THE SOUND SHIELDING BY BUILDINGS

The fundamental facts for the calculation procedure are as follows.

The pattern of the sound field at a succeeding corner coming from the scattering at the preceding corner is similar to that of a line source of approximate strength at the preceding corner.

Except for sources very near to the horizon the level on the second flank steeply decreases within a small distance from the corner at which scattering takes place. Therefore, multiple scattering between succeeding and preceding corners generally can be neglected.

The sound field is reciprocal with respect to ϑ and ϑ_q.

The computations above require knowledge of the sound pressure of the source $|p_Q(0)|$ at the scattering corner.

The determination of the noise shielding by buildings proceeds as follows.

Determine the wave number k_z (if any) and with that the radial wave number k from equation (3).

Decide whether the real source should be modelled by a plane wave (then determined ϑ_q relative to the second flank of the first corner) or by a line source (then determine r_q and ϑ_q).

Determine the sound pressure $|p_{Q1}(0)|$ of the source at the first corner.

Compute the sound pressure level $L_2(kb, 0)$ at the second corner (see Figure 1 for b).

Assume a line source in the first corner which produces the source level $20 \lg (|p_{Q2}(0)|) = L_2(kb, 0)$ at the second corner.

Repeat the scattering calculation at the second corner with this $|p_{Q2}(0)|$: i.e., measure the source and receiving point angles from the second flank of the second corner and compute $L_3(kr, 0)$ in the third corner (if a third corner must be considered, with r = distance between the second and third corners) or compute $L_3(kr, \vartheta)$ if the second corner is the last corner (then r is the distance between this last considered corner and the receiving point and ϑ the angle between the last flank and the receiving point).

Continue the procedure for the sequence of corners which must be considered.

The final result will give the sound pressure level at the receiving point relative to the pressure $|p_{Q1}(0)|$ of the original source in the first corner. The assumed condition is a totally absorbing ground below the receiving point. If the receiving point is near to a reflecting ground, add $10 \lg (1 + |r|^2)$ to the computed level with $|r|$ the reflection coefficient of the ground. If the receiving point is at some distance above the ground, then repeat the last step of the procedure with r, ϑ the radius and angle to the mirror-reflected (at the ground plane) receiving point. Add the two contributions (magnitudes of sound pressure) with the second one multiplied with $|r|$.

Depending on the local situation (height and length of the building), the procedure must be repeated for the sound paths *over* the building and *around* the building. It is evident that in practical applications the single corner scattering must be computed very often. The computations can be reduced to the evaluation of $L(kr, 0)$ because of the reciprocity of the field behind a corner with respect to ϑ and ϑ_q. Therefore, in the next section, a method is derived for a fast computation

of $L(kr, 0)$. The use of $L(kr, 0)$ for the evaluation of $L(kr, \vartheta)$ (called $L_3(kr, \vartheta)$ in the above description) shall be explained here in more detail.

As Figure 13 illustrates, the scattering at building corners (in the example shown, with two corners) can be composed—under the conditions mentioned above—by a repeated single corner scattering. The last corner generally is associated with a non-zero receiver point angle ϑ_2, whereas in the preceding scattering evaluations the receiver point angles were $\vartheta = 0$: i.e., it was sufficient to evaluate $L(kr, 0)$. However, $L(kr, 0)$ will be the main part of the evaluation in the last scattering also, if one makes the exchanges $\vartheta \leftrightarrow \vartheta_q$, $r_2 \leftrightarrow r_{q2}$ and keep $p_{Q2}(0)$ (the result of the preceding evaluation) constant, as is indicated by the transition from the second to the third line in Figure 13. At the same time one has to exchange the equations, (18a) $\leftrightarrow$ (18b) (first sums only). One evidently will obtain the wanted level at the receiving point P when one adds to the lastly determined $L(kr, 0)$ (with a fictitious source at P) the term $20 \lg |H_0^{(2)}(kr_2)/H_0^{(2)}(kr_{q2})|$. Because

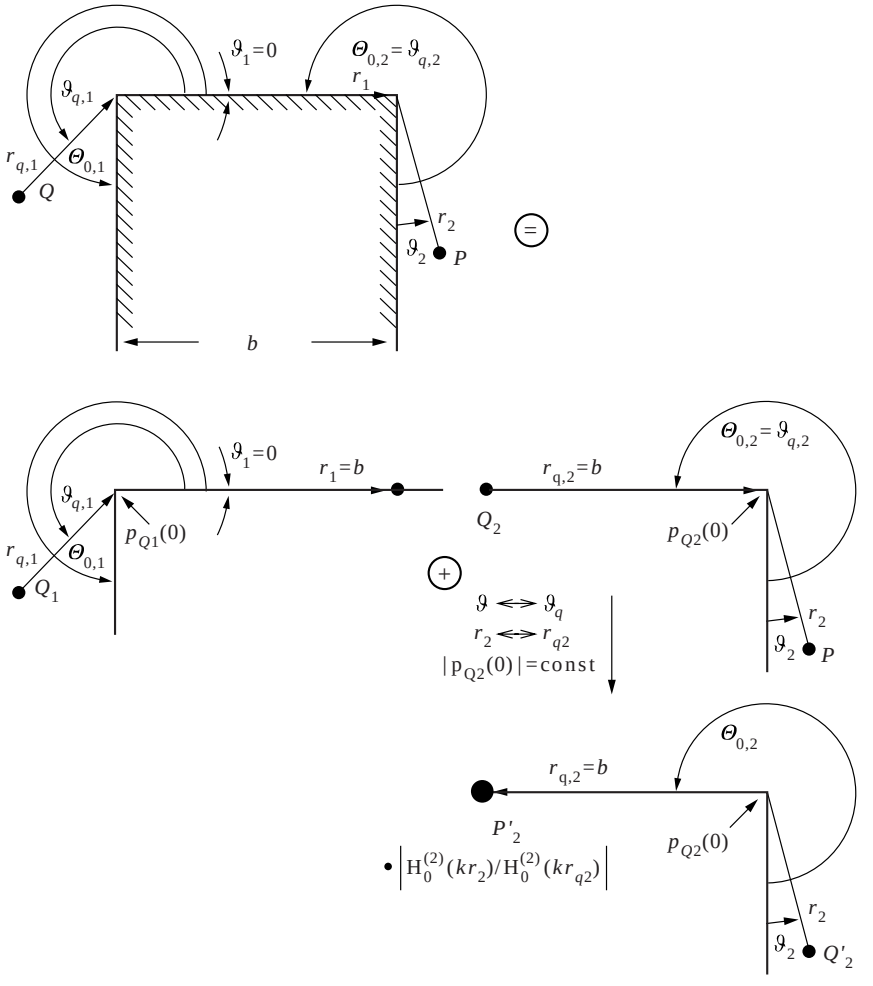

Figure 13. How the evaluation for the scattering at two succeeding corners can be reduced to the repeated evaluation of $L(kr, 0)$.

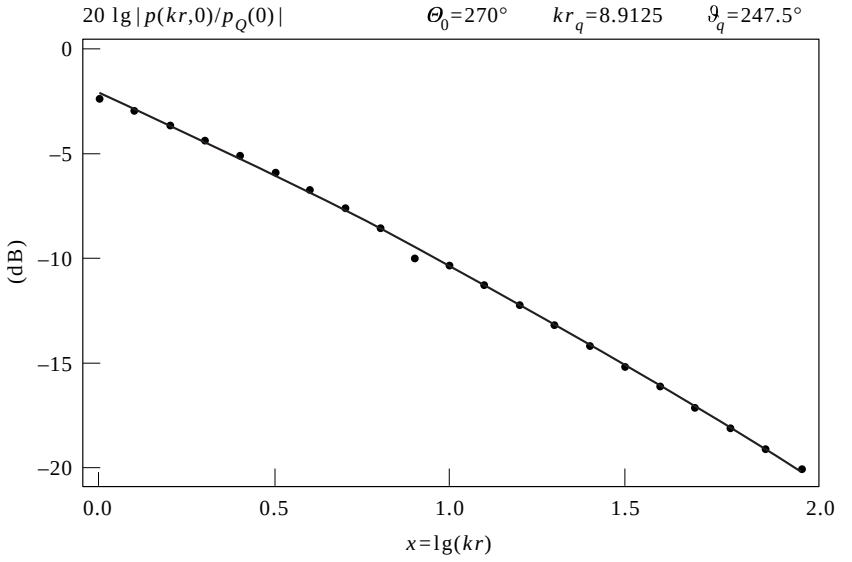

Figure 14. Example for the polynomial approximation (curve) to the sound pressure level $L(kr, 0)$ at the second flank of a right-angled corner for a line source with $kr_q \approx 8{\cdot}913$, $\vartheta_q = 247{\cdot}5^\circ$. Comparison with results of the analytical evaluation (points).

the ratio of magnitudes of Hankel functions of order zero equals the root of the reciprocal ratio of their arguments, $L(kr, 0)$ indeed is the main part of the last scattering evaluation also.

9. SIMPLIFIED COMPUTATION OF $L(kr, 0)$

The quantity $L(kr, 0)$ is the sound pressure level on the second flank of a corner at a point a distance r from the scattering corner. The variable used for this quantity is kr. It depends on the parameters of the wedge angle Θ_0 and of the source position parameters kr_q, ϑ_q in the case of a line source, and of the wave direction ϑ_q for an incident plane wave. An implicit parameter is the source strength $|p_Q(0)|$ at the scattering corner.

$L(kr, 0)$ was computed for kr stepping through $1 \leqslant kr \leqslant 100$ with a step $\Delta \lg(kr) = 0{\cdot}1$ (i.e., with about one-third octave steps). The sampling points for the parameters with $\Theta_0 = 270^\circ$ and $\Theta_0 = 360^\circ$ were $180^\circ \leqslant \vartheta_q \leqslant \Theta_0$ with $\Delta\vartheta_q = 7{\cdot}5^\circ$ and $\Delta\vartheta_q = 3{\cdot}75^\circ$ for $\Theta_0 = 225^\circ$. The source distance kr_q (for a cylindrical wave) was taken midway between the sampling values of kr. The computation time was 7·2 h for a cylindrical wave and 1·25 h for a plane wave.

The simplification begins with a polynomial least squared error fit to $L(kr, 0)$:

$$L(kr, 0) = a_0 + a_1 x + a_2 x^2 + \cdots, \qquad x = \lg(kr)$$

$$a_i = \begin{Bmatrix} a_i(\Theta_0, kr_q, \vartheta_q) \\ a_i(\Theta_0, \vartheta_q) \end{Bmatrix}, \qquad i = \begin{Bmatrix} 0, 1, 2, & \text{line source} \\ 0, 1, 2, 3, & \text{plane wave} \end{Bmatrix}. \tag{22}$$

TABLE 1

(*a*) *Coefficients* $b_{m,n}(\Theta_0,i)$ *of equation* (24*a*) *with a line source and two wedge angles* $\Theta_0 \neq 2\pi$

	$\Theta_0 = 270^\circ$			$\Theta_0 = 225^\circ$		
	a_0	a_1	a_2	a_0	a_1	a_2
$b_{0,0}$	−3·508914089	−8·048512868	−0·6310612470	−0·09540693872	−7·3238335049	−0·8765745279
$b_{1,0}$	2·522196950	−0·009541528038	−0·1423972091	3·1825983742	3·0205071852	−1·2033629841
$b_{2,0}$	−1·883348105	0·5769454995	0·01678228228	−2·2114376268	−0·08553799890	0·3513458955
$b_{3,0}$	0·4967954203	−0·3051673769	0·04756468413	0·5797754874	−0·4849823570	0·03401430131
$b_{0,1}$	0·02544989020	0·3821548481	−0·1407494337	−1·521470673	3·2843166927	−1·5290120909
$b_{0,2}$	0·8345544874	0·2651097458	−0·08464913202	2·9650638176	−4·2599417741	1·9733888600
$b_{1,1}$	0·3679533261	−0·6159740550	0·5043646313	3·5125797465	−7·6016950005	4·0117267131
$b_{1,2}$	0·3777082514	3·292101514	−1·107819931	−4·4380492254	16·5213645840	−7·3478392442
$b_{2,1}$	−0·09024391927	0·2958236606	−0·7181971540	−1·7393927223	4·2761593211	−2·3524985081
$b_{2,2}$	−0·1947245060	−0·8724895618	0·8256508092	2·1463076803	−7·4133414548	4·8096517591

(*b*) *Coefficients* $b_{m,n}(\Theta_0, i)$ *of equation* (24*b*) *with a line source and the wedge angle* $\Theta_0 = 2\pi$

	$\Theta_0 = 360^\circ$		
	a_0	a_1	a_2
$b_{0,0}$	−9·0746493294	−8·7968786424	−0·4550505284
$b_{1,0}$	1·3520538823	−0·4605118745	0·1300965967
$b_{2,0}$	−1·1527527549	0·2689865167	−0·06995829336
$b_{3,0}$	0·3306858082	−0·03586357874	−0·03107882535
$b_{0,1}$	−0·1455294858	0·6092864775	−0·2438201115
$b_{0,2}$	0·5960196681	0·8416378006	−0·3079336093
$b_{0,3}$	−0·008012063348	0·1356184578	−0·05023497076
$b_{1,1}$	0·6291707040	−1·5301268286	0·7849193467
$b_{1,2}$	0·8532798218	−1·5894224358	0·7181240230
$b_{1,3}$	0·1325783868	−0·6606164056	0·2441835343
$b_{2,1}$	−0·2481813528	0·7158176859	−0·7782697727
$b_{2,2}$	−0·3078462069	0·6233222389	−0·7604596554
$b_{2,3}$	−0·04647002117	0·2175905849	−0·2139967639

TABLE 2

Coefficients $b_m(\Theta_0, i)$ of equation (25) with a plane wave and different wedge angles Θ_0

	a_0	a_1	a_2	a_3
$\Theta_0 = 270^\circ$				
b_0	−2·3897749010	−6·3871816950	−2·5521245973	0·5883191145
b_1	−0·1395262072	1·4298990382	−2·3420050592	0·7953788225
b_2	2·4146524033	−6·2941352347	14·7867785184	−5·5243620562
b_3	−2·0826383489	22·1143696537	−38·0273605653	13·7842093181
b_4	1·7277125263	−19·7690393085	36·1731866937	−13·6837211307
b_5	−0·5024423058	5·5652217504	−10·7284415031	4·3492902596
$\Theta_0 = 225^\circ$				
b_0	1·5680782122	−3·0816597309	−3·7292266269	0·671069424680
b_1	0·04605330206	−0·5413285417	1·0808880010	−0·5457149106
b_2	0·9901780451	8·6690503927	−4·0768626382	3·3222271919
b_3	1·8882278171	−24·2944777516	52·4234791286	−28·5329448742
b_4	−1·2048732997	19·7879485353	−59·9341011899	41·1343130200
b_5	−0·5572513587	0·7720284647	11·3285552296	−13·87141596900
$\Theta_0 = 360^\circ$				
b_0	−8·6190291475	−8·4954146753	−1·0515339568	0·2143116375
b_1	−0·04914242523	0·6349841469	−2·3970346444	1·3968013166
b_2	0·9889355168	−0·9414382840	6·1112326674	−3·9023864807
b_3	−0·09677973083	0·9074414634	−5·9035085751	3·9492264464
b_4	0·04314542296	−0·03120088534	2·0087474020	−1·5499399018
b_5	−0·007092745198	−0·03111306942	−0·2088099622	0·2033883155

A squared polynomial turned out to be sufficient with a line source, and a cubic polynomial with an incident plane wave. Figure 14 shows a typical example for the fit of the polynomial curve to the points from the analytical evaluation. The least squared error fit widely eliminates the numerical errors at $kr \approx kr_q$ of the analytical evaluation. The coefficients $a_i(\Theta_0, kr_q, \vartheta_q)$ were determined for all parameter combinations.

As a next step the coefficients a_i with a line source were represented as functions of $z = \lg(kr_q)$ by a polynomial:

$$a_i(kr_q) = c_0 + c_1 z + c_2 z^2 + c_3 z^3, \qquad z = \lg(kr_q),$$

$$c_j = c_j(\Theta_0, \vartheta_q, i), \qquad j = 0, 1, 2, 3. \tag{23}$$

Figure 15. (a) Example for the complete polynomial approximation (curves) to the sound pressure level $L(kr, 0)$ at the second flank of a right-angled corner for a line source with small source distance $kr_q = 1{\cdot}122$ and different source angles ϑ_q; comparison with results of the analytical evaluation (point). (b) Comparison of the complete polynomial approximation (curves) with results of the analytical evaluation (points) as in (a), but for medium source distance $kr_q = 8{\cdot}913$. (c) Comparison of the complete polynomial aproximation (curves) with results of the analytical evaluation (points) as in (a), but for large source distance $kr_q = 70{\cdot}79$.

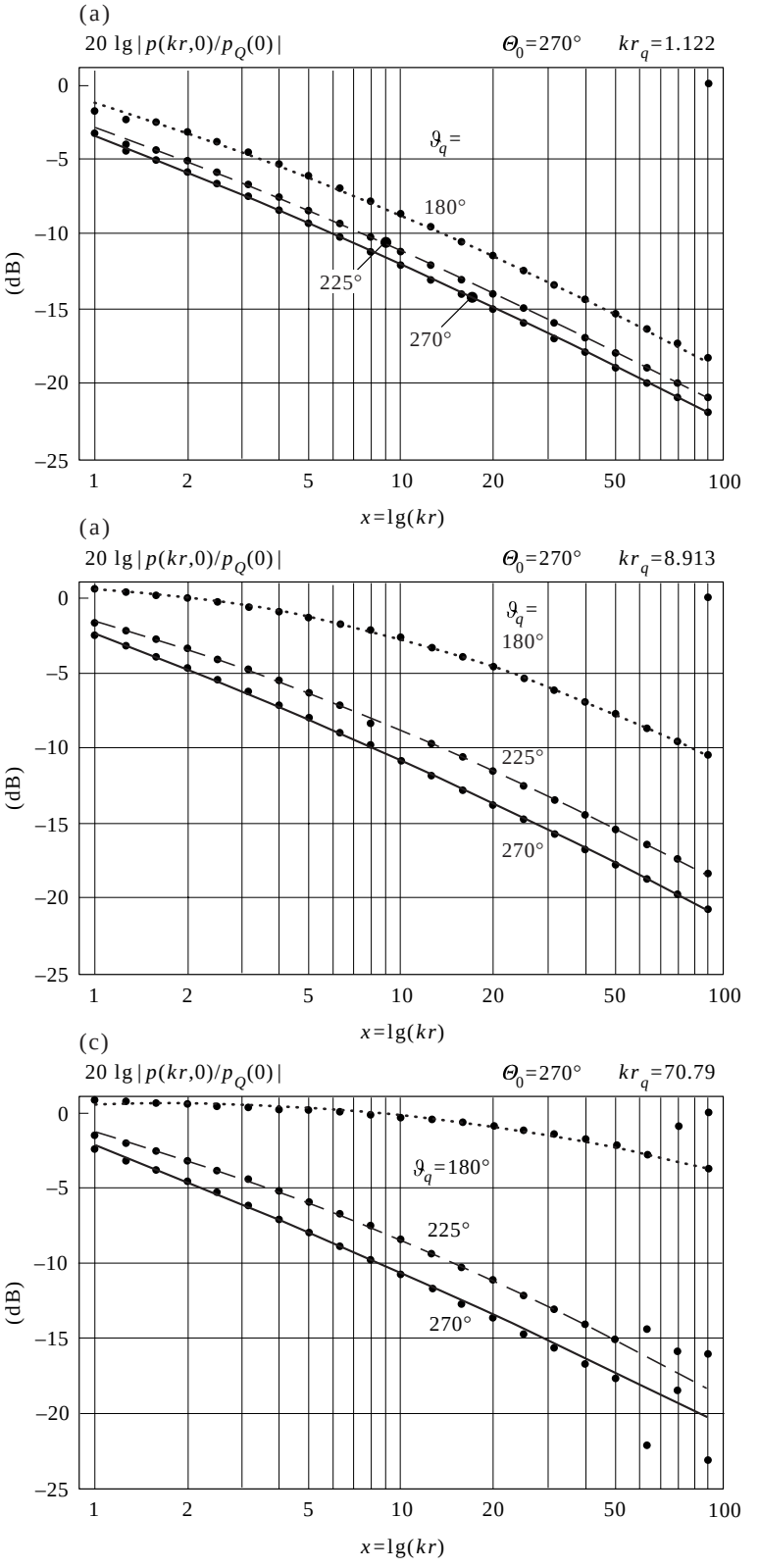

Figure 15—(*Caption opposite*).

A cubic polynomial was necessary for a sufficient precision (errors below 1/2 dB between the analytical and approximated values of $L(kr, 0)$). This procedure did end here, because it was not possible to find a simple representation of the coefficients c_j as a function of ϑ_q. Because 12 numerical coefficients c_j would be needed for every parameter value of ϑ_q, lists of these coefficients for enough ϑ_q values would become voluminous.

Therefore, a two-dimensional regression of the coefficients $a_i(\Theta_0, kr_q, \vartheta_q)$ as functions of $z = \lg(kr_q)$ and $y = (\Theta_0 - \vartheta_q)_{\text{rad}}$ was applied (the angular unit in radians is used in order to make the ranges of z and y of similar size, which permits one to estimate which terms in a polynomial are needed). The finally used representation of the coefficients a_i with a line source generally has the shape

$$\begin{aligned} a_i(kr_q, \vartheta_q) &= b_{0,0} + b_{1,0}z + b_{2,0}z^2 + b_{3,0}z^3 + b_{0,1}y + b_{0,2}y^2 \\ &\quad + b_{1,1}zy + b_{1,2}zy^2 + b_{2,1}z^2y + b_{2,2}z^2y^2, \\ z = \lg(kr_q); \qquad y &= (\Theta_0 - \vartheta_q)_{\text{rad}}; \qquad i = 0, 1, 2, \text{ line source}, \\ b_{m,n} &= b_{m,n}(\Theta_0, i), \qquad \Theta_0 \neq 2\pi, \end{aligned} \tag{24a}$$

and in the special case of a line source and $\Theta_0 = 360^\circ$ (notice the change in y),

$$\begin{aligned} a_i(kr_q, \vartheta_q) &= b_{0,0} + b_{1,0}z + b_{2,0}z^2 + b_{3,0}z^3 + b_{0,1}y + b_{0,2}y^2 + b_{0,3}y^3 \\ a_i(kr_q, \vartheta_q) &= b_{0,0} + b_{1,0}z + b_{2,0}z^2 + b_{3,0}z^3 + b_{0,1}y + b_{0,2}y^2 + b_{0,3}y^3 \\ &\quad + b_{1,1}zy + b_{1,2}zy^2 + b_{1,3}zy^3 + b_{2,1}z^2y + b_{2,2}z^2y^2 + b_{2,3}z^2y^3, \\ z = \lg(kr_q), \qquad y &= (\vartheta_q - \Theta_0)_{\text{rad}}, \qquad i = 0, 1, 2, \text{ line source}, \\ b_{m,n} &= b_{m,n}(\Theta_0, i), \qquad \Theta_0 + 2\pi. \end{aligned} \tag{24b}$$

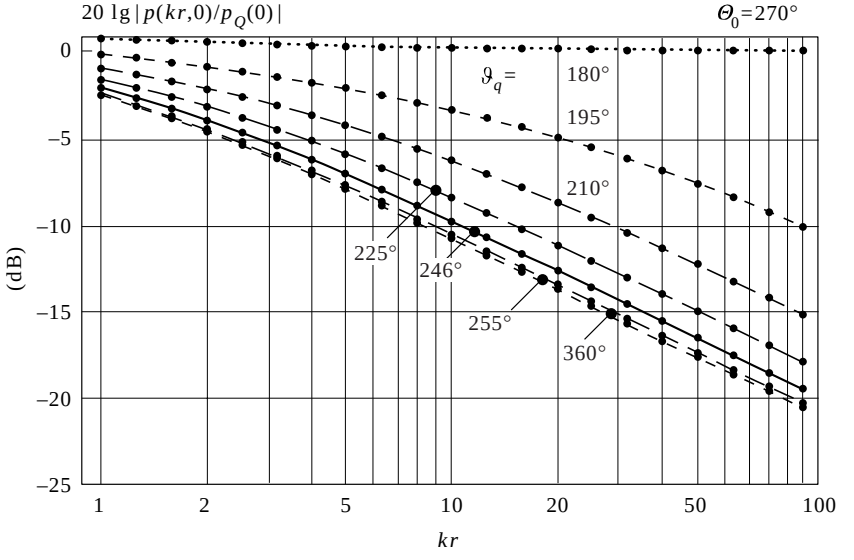

Figure 16. Comparison of the complete polynomial approximation (curves) to results of the analytical evaluation (points) of the sound pressure level $L(kr, 0)$ at the second flank of a right-angled corner for a plane wave incident under different source angles ϑ_q.

The line source associated with $\Theta_0 = 360^\circ$ is treated as a special case, because the screen effectively does not exist for source angle values $\vartheta_q = 180^\circ$ and near to that; the dominant source is the original source and not the scattering corner. This fact makes necessary a special treatment.

The coefficients a_i with an incident plane wave are computed with the polynomial approximation

$$a_i(\vartheta_q) = b_0 + b_1 y + b_2 y^2 + b_3 y^3 + b_4 y^4 + b_5 y^5,$$

$$y = (\Theta_0 - \vartheta_q)_{\text{rad}}, \qquad i = 0, 1, 2, 3, \text{ plane wave}, \qquad b_m = b_m(\Theta_0, 0). \tag{25}$$

The values of the coefficients $b_{m,n}$ for equation (24a) are shown in Table 1(a), and for equation (24b) in Table 1(b), both for excitation by a line source. The coefficients for equation (25) for plane wave incidence are given in Table 2.

Figures 15(a, b, c) compare so computed curves of $L(kr, 0)$ with points from the analytical evaluation for line sources with small $kr_q = 1{\cdot}122$, medium $kr_q = 8{\cdot}913$ and rather high $kr_q = 70{\cdot}79$, respectively, with the values $\vartheta_q = 180, 225, 270^\circ$ in each diagram. The error is smaller than about 1/2 dB; one can see how the approximations eliminate the errors in the analytical evaluation at $kr = kr_q$ (especially with large kr_q values). Figure 16 shows curves for an incident plane wave computed with the approximation and compares with points from the analytical evaluation. The errors are below about 0·25 dB. The application of the polynomial approximations is restricted to the range $1 \leqslant k \leqslant 100$, $1 \leqslant kr_q \leqslant 100$, $180^\circ \leqslant \vartheta_q \leqslant \Theta_0$.

10. CONCLUSION

Analytical expressions have been given for the sound field around a rigid corner which is excited either by a line source or by an incident plane wave. The expressions are based on a field analysis with wedge modes. It has been shown that under most practical conditions multiple scattering between succeeding corners can be neglected. This and the fact that the sound field at the shadow flank has an azimuthal pattern like the field of a line source permits an easy evaluation of the noise shielding by buildings. It has been shown how these computations can be reduced to the evaluation of the level $L(kr, 0)$ at shadow flanks. Simple polynomial approximations are given for $L(kr, 0)$, the precision of which is high enough for noise control predictions.

REFERENCES

1. F. P. Mechel 1998 *Journal of Sound and Vibration* **216**, 649–671. Modes in lined wedge-shaped ducts.
2. F. P. Mechel 1998 *Journal of Sound and Vibration* **216**, 673–696. Modal analysis in lined wedge-shaped ducts.
3. International Standard ISO/DIS 9613-2, Acoustics—attenuation of sound during propagation outdoors—Part 2: a general method of calculation; Verein Deutscher Ingenieure VDI, Guidelines VDI 2720, Schallschutz durch Schirmung; Verein Deutscher Ingenieure VDI, Guidelines VDI 2714, Schallausbreitung im Freien.

4. M. Möser 1995 *Acustica* **81**, 565–586. Die Wirkung von zylindrischen Aufsätzen an Schallschirmen.
5. F. P. Mechel 19XX *Schallabsorber*. Stuttgart: S. Hirzel. See volume III, chapter 23: Schallschirm mit absorbierendem Zylinder-Aufsatz.